



## Coupled dynamic modelling of moored floating structure

E. Gücüyen<sup>1,\*</sup>, R. T. Erdem<sup>2</sup>

### ARTICLE INFO

#### Article history:

Received 16 Aug 2024;  
in revised from 20 Aug 2024;  
accepted 17 Sep 2024.

#### Keywords:

Floating body; Free surface simulation;  
Numerical analysis; Wave  
environment.

### ABSTRACT

This paper is aimed to explore the effects of the wave directions and mooring lines on the dynamic characteristics of the semi-submersible offshore platform. The coupled numerical analysis is generated between the platform motions, the mooring lines and the marine environment. Four column semi-submersible platform serves as a floating body, four mooring lines and the wave environment constitutes the numerical model. Wire elements with different slack-taught types are utilized in modelling the mooring lines. On the other hand, the platform is considered as a rigid body having six degrees of freedom (6 DOF) motions. Several wave incidence directions are used to symbolize the marine environment. Besides, tensions of the mooring lines as well as the motions of the platform that changes by time are determined according to different configurations of the mooring lines and directions of the waves. Bidirectional fluid structure interaction analysis is performed to obtain the most critical results among the configurations and the directions. Fully nonlinear free surface simulation is carried out due to the Coupled Eulerian Lagrangian (CEL) analysis that is generated by the finite elements method and the results are compared with the results determined from analytic solution of free surface elevations.

© SEECMAR | All rights reserved

### 1. Introduction.

Fully submerged or semi submerged floating structures can be used as solar, wind and wave energy harvesting structures (Han et al. 2020; Xu et al. 2021; Chandrasekaran, and Sricharan 2020), breakwater (Ji et al. 2016), fish farming site (Jim et al. 2021), transportation facility (Xia et al 2019, Manisha, Kaligatla and Sahoo 2019) and offshore barrier structure (Aboshio and Ye 2016).

Generally, floating structures are comprised of superstructure, floaters, mooring lines and anchorages. The superstructure could be a truss system, single pile or a different type of structure, depending on the intended use of the structure. Stability of the superstructure can be provided by mooring lines, ballasts and pontoons. Although all of these can be utilized to-

gether, stability can also be provided by coupling of mooring lines-ballasts mooring lines-pontoons.

Mooring lines are the main components in the floating structures and represent a remarkable part of the project cost. Mooring lines are studied according to arrangements, material properties and slack-taut process in the literature. In the study of Jin et al. (2020) two different mooring designs are considered; in the first design stiff mooring line and in the second design three times stiffer than first design is utilized. The effects of mooring stiffness on the nonlinear behavior are checked. Different positions of the mooring lines experimentally are investigated by Gomes et al. (2020). The study examines the performance of a single isolated device, an array with independently-moored devices and three arrays with inter-body connections, with different levels of connectivity in the mooring arrangement. Different mooring line arrangements are modelled by Huang et al. (2020). The mooring force of the fish farm in the waves has been measured and compared for different single-point mooring arrangements. Therefore, a safe and reliable mooring form is selected as the mooring system for this farm. Yuan et al (2014) modelled the moorings in two different ways; taut and hybrid mooring to determine the motion responses of a semi-

<sup>1</sup>Professor of Civil Engineering Department of Manisa Celal Bayar University, Turkey.

<sup>2</sup>Professor of Civil Engineering Department of Manisa Celal Bayar University, Turkey.

\*Corresponding author: E. Gücüyen, Tel. (+090) 2362012321. E-mail Address: [engin.gucuyen@cbu.edu.tr](mailto:engin.gucuyen@cbu.edu.tr).

submersible. Slack-taut mooring system is created by Qiao et al (2020) to analyse the motions of the mooring line affected by hydrodynamic load of mooring line by performing numerical analysis. Twelve mooring lines produced of chain-polyester rope-chain combination are used in performance simulation of coupled hull-mooring-riser system in the study of Chung, Kang and Kim (2020). Out of plane bending, interlink angles, bending moments, and accumulated fatigue damages are obtained in this study.

Hermawan and Furukawa (2020) have divided the mooring chains in three segments that have various material characteristics and length so as to attain the enough tension and cost efficiency of the mooring line of the offshore structure. Beside this, the effect of the directions of external forces on the structure is considered in the same study.

Floating structures are considered as complex structures across waterbodies exposed to several load effects. The major environmental forces acting on the floating offshore structures are; wave, current and wind forces whose effect is taken into account with the increasing building height. A study has been performed about incidence angles of these forces by Li et al (2020). The authors have used a limited number of wind-wave misalignment  $\beta$  and the yaw error to reveal that the motions of the platform are significantly influenced by the wind-wave directions. In the experimental study of Chen, Chen and Yun-Xiang (2020) it is aimed to analyse the forces acting on the semi-submersible with six different propagation directions. In the study of Zhou et al (2017) the directionality effects of aligned wind and wave load on the dynamics of the triangular semi-submersible foundation are discussed. The load cases reveal that hydrodynamic forces lead to the directionality distinctions for surge and pitch, tower base bending moments as well as nacelle accelerations.

The mooring system can affect the motions of the floating elements, so that the coupled analysis between the motions of floating elements and the mooring forces is necessary. Wiegard et al (2019) have presented coupled fluid-structure interaction simulation to analyse the motion behaviour, stresses and deformations of a floating wind turbine. Intact and sub-structuring finite element model are comparatively studied to detect the behavior of the coupled structure. Chen et al (2017) have carried out hydrodynamic analyses of a moored floating pontoon via numerical simulations and experiments. The history curves of motions of the pontoon are comparatively studied by numerically and experimentally. Besides that time varying mooring forces in four different wave directions and in three wave amplitudes are obtained to determine wave influences on the mooring lines. In the study of Ji et al. (2017) geometrical property of the structure and wave condition effects on the motion responses of the moored breakwater are investigated by means of experiments and numerical models. Coupled-Eulerian Lagrangian method is adopted in the numerical part of the study achieve the sway, heave and roll motions of the breakwater.

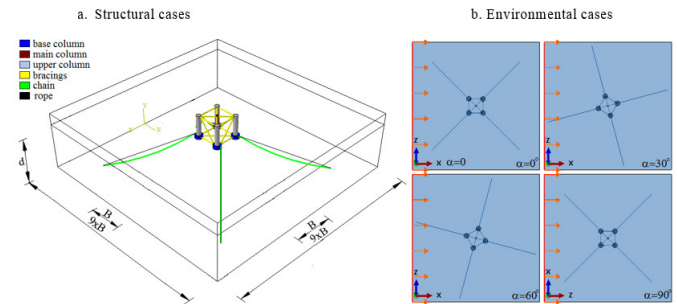
In the literature survey, it is seen that numerical and experimental (Haicheng et al., 2018; Rajeswari and Nallayarasu, 2021; Gücüyen and Erdem, 2022) methods are usually used to model the dynamic behavior of the infrastructure of the float-

ing typed turbine. In this study, dynamic behaviour of a semi-submersible typed structure and mooring lines in different wave incoming directions is numerically analyzed. In addition, effect of mooring lines on the structural behaviour is investigated. CEL technique is utilized by Abaqus software in the numerical analysis. Sway, heave, and roll displacements of the structure and tensions of the moorings are determined according to different wave loading and mooring line conditions. Therefore, the effect of different wave directions and mooring lines on the behavior of the floating structure is determined in the end.

## 2. Structural and Environmental Cases.

Four column semi-submersible platforms with two different mooring line designs have been generated under four wave directions ( $\alpha$ ). Thus, a total of 8 different cases have been investigated. Structural and environmental cases are presented in Figure 1.

Figure 1: Coupled models and cases.



Source: Authors.

Figure 1.a. shows the structural situations where different rope types are used. In addition, dimensions of the marine environment determined according to the size of the structure are seen in the same figure. Figure 1.b. shows the position of the structure according to wave incidence angles. Description of the structural and environmental cases in Figure is given in Table 1.

Table 1: Description of the cases.

Case type	structural cases		Case type	environmental cases			
	slack	taut		Incident angle	$\alpha=0$	$\alpha=30$	$\alpha=60$
Mooring line design	SC-1	SC-2	Case name	EC-1	EC-2	EC-3	EC-4

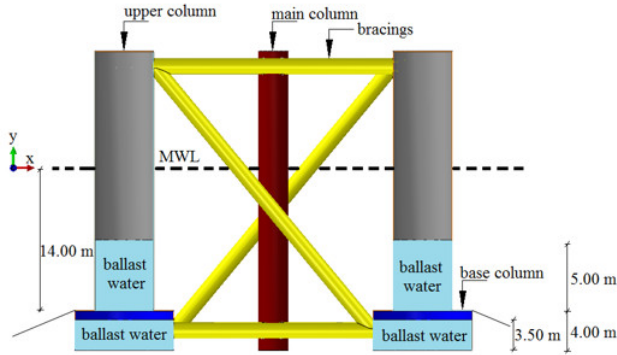
Source: Authors.

### 2.1. Structural cases.

Semi-submersible platform contains four offset columns, a main column, and bracing components as it is seen in Figure 1.a. Base and upper column constitute the offset column. Main column is located at the centre of the platform that supports the wind turbine which has a diameter of 3 m, a length of 30 m and

thickness of 0.03 m. The diameter, length and thickness of the upper columns are 6 m 26 m and 0.06 m, respectively. The base columns, kept under the upper columns, have a diameter of 10 m a length of 4 m and thickness of 0.06 m. Spacing between base columns (B) is 30 m. The diameter and the thickness of the bracings are 1.6 m and 0.0175 m respectively. Steel material is used for all components with Young's modulus of  $2.1 \times 10^{11}$  N/m<sup>2</sup>, density of  $7.85 \times 10^3$  kg/m<sup>3</sup>, and Poisson ratio of 0.3.

Figure 2: Layout of the platform.



Source: Authors.

The structure is ballasted with water, density of 1025 kg/m<sup>3</sup>, in the offset columns. The water is compartmented and is not permitted to act and slosh. The four upper columns are filled with water from the bottom up to 5.00 m, and the base columns are filled from bottom up to 3.50 m, as it is shown in Figure 2. Depth of fairleads below mean water level (MWL) is 14 m. Ballasted mass of the platform is  $3.66 \times 10^6$  kg. Location of centre of mass is 9.28 m below MWL. Roll inertia is  $1.08 \times 10^9$  kgm<sup>2</sup>, yaw inertia is  $1.08 \times 10^9$  kgm<sup>2</sup> and pitch inertia is  $1.29 \times 10^9$  kgm<sup>2</sup>. Spacing between offset columns (B) is 30 m. The distance between MWL and the platform base is 18 m where the water depth (d) is 60 m.

Same floating platform is used in two structural cases. The cases are determined according to mooring lines being slack or taut. While steel-chain lines are used in slack case (SC-1), polyester rope lines are used in taut case (SC-2). The values of geometrical and material properties that are used in the study are given in Table 2.

Table 2: Properties of mooring lines.

Property	Value of chain	Value of rope
Length (m)	142	119
Diameter (m)	0.147	0.175
Density (kg/m <sup>3</sup> )	8000	1270.29
Young's Modulus (Pa)	$2.09 \times 10^{11}$	$1.2473 \times 10^{10}$

Source: Authors.

## 2.2. Environmental cases.

The marine environment of the structure is generated with wave forces. Velocity profile of Linear Wave Theory is utilized to model the wave that is seen in Eq. (1). This equation is used for inlet velocity equation of wave in numerical analysis.

$$u = \frac{H}{2} \frac{gT}{L_w} \frac{\cosh[2\pi(y+d)/L_w]}{\cosh(2\pi d/L_w)} \cos\left(\frac{2\pi}{L_w}x - \frac{2\pi}{T}t\right) \quad (1)$$

In the equation, H symbolizes the wave height, T represents the wave period, g shows the gravity,  $L_w$  represents the wave length, d is the water depth, t symbolizes the time, x and y shows the horizontal and vertical positions respectively. The marine environment is ensured by considering  $d=60$  m,  $T=6$  s and  $H=4$  m. Wave length ( $L_w$ ) is determined as 56.20 m by using these values.

Surface simulation of marine environment is simulated by CEL analysis and the results are compared with results are obtained from analytic solutions. Equation of surface elevation that is used in comparison is given by the following equation.

$$\eta = \frac{H}{2} \cos\left(\frac{2\pi z}{L_w} - \frac{2\pi t}{T}\right) \quad (2)$$

## 3. FSI Analysis.

Lagrange and Eularian procedures are followed through CEL technique in the numerical analysis. This technique is explained in the sections below.

### 3.1. Formulation of CEL Technique.

Formulation of CEL technique that is utilized by the software is described by the equations below. Eqs. (3-5) are the mass, momentum and energy Lagrangian conservation equations. In the equations  $v$ ,  $\rho$ ,  $\sigma$ ,  $b$  and  $e$  symbolize material velocity, density, the Cauchy stress, the body force and the internal energy per unit volume respectively.

$$\frac{D\rho}{Dt} + \rho \nabla \cdot v = 0 \quad (3)$$

$$\rho \frac{Dv}{Dt} = \nabla \cdot \sigma + \rho b \quad (4)$$

$$\frac{De}{Dt} = \sigma : D \quad (5)$$

The general conservation form of governing equations for Lagrangian technique are obtained by Eq. (6), for Eularian procedure as follows.

$$\frac{D\varphi}{Dt} = \frac{\partial \varphi}{\partial t} + v \cdot (\nabla \varphi) \quad (6)$$

$$\frac{\partial \varphi}{\partial t} + \nabla \cdot \Phi = S \quad (7)$$

$\varphi$  represents the arbitrary solution variable,  $\Phi$  symbolizes the flux function and S is the source term in the Eq. (7).

$$\frac{\partial \varphi}{\partial t} = S \quad (8)$$

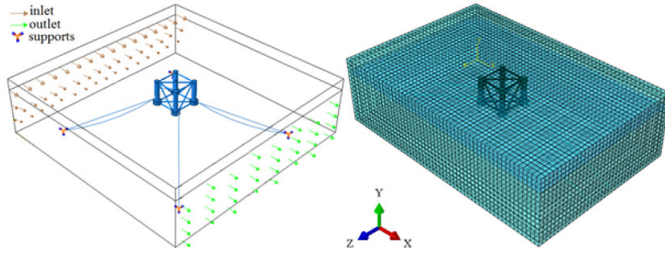
$$\frac{\partial \varphi}{\partial t} + \nabla \cdot \Phi = 0 \quad (9)$$

Eq.(8) is the same with the standard Lagrangian formulation in case the spatial time derivative is changed by the material time derivative on the fixed mesh. The deformed mesh is transferred to the original fixed mesh. Afterwards, volume of the material transferred between the adjacent elements is determined to solve the Eq. (9).

### 3.2. Creating the Models by CEL Analysis.

Finite element model of the SC-2 / EC-1 is seen in Figure 3. The right side of the figure reveals the marine environment constituting the Eulerian part and structure generating the Lagrangian part.

Figure 3: Schematic view of the model.



Source: Authors.

Material characteristics of the Lagrangian part have been explained in Section 2.1. The environment of the structure is modelled as EOS materials with the velocity of sound ( $c_0$ ) in salty water 1560 m/s, with the density ( $\rho$ ) of 1025 kg/m<sup>3</sup> and the dynamic viscosity ( $\mu$ ) of 0.0015 Ns/m<sup>2</sup>. In addition, void depth is taken as 15 m and the water depth ( $d$ ) is 60 m in the numerical model. In the next step, the load and the boundary conditions are defined. Direction of flow belonging to Eulerian part is seen in Figure 3. An outlet boundary condition is indicated at the opposite side of the inlet, bottom of marine region is set to wall boundary condition where all of the velocity components are zero. The far field boundary condition is assigned to side walls where velocity is assumed to be equal to inlet velocity. A few trials have been made to decide the most proper finite element size via natural frequency values in Abaqus by using Lanczos method. The spectral transformation is employed by the Lanczos procedure that is found in the software. Eq. (10) is implemented to Eq. (11) where  $k$  and  $m$  are the stiffness and mass matrix respectively. In addition,  $\omega$  symbolizes the square of natural frequency,  $\sigma$  represents the shift,  $\theta$  is the eigenvalue, and  $\xi$  indicates the eigenvector [30].

$$[m] ([k] - \sigma[m])^{-1} [m] \{\xi\} = \theta [m] \{\xi\} \quad (10)$$

$$(-\lambda [m] + [k]) \{\xi\} = 0 \quad (11)$$

As it is seen in Figure 3, three dimensional, 8-node linear brick, hexahedron element type (C3D8R) and linear line elements of type B31 are utilized in the modelling stage. Natural frequency of sway mode values for various number of nodes and elements are presented in Table 3 for SC-2.

Table 3: Numerical values by mesh size.

Mesh size (m)	Node number		Element Number		Natural Frequency (rad/s)	Change between the rows (%)
	Mooring Lines	Floating Structure	Mooring Lines	Floating Structure		
0.15	3184	273201	3180	276421	0.243	18.12
0.10	4772	605020	4768	610807	0.205	15.04
0.075	6364	1068840	6360	1078122	0.179	2.97
0.05	9544	2432699	9540	2451377	0.173	1.07
0.025	19080	11124142	19076	11258260	0.171	

Source: Authors.

As the mesh size is decreased from 0.075 to 0.025, the difference between natural frequency values is calculated as 4.67% according to Table 3. So, mesh size is determined as 0.075 m for the Lagrangian part in the end. Therefore, 125480 number of nodes and totally 117056 number of elements have been utilized. Between these elements, B31 type 1496 ones belong to mooring line and C3D8R type 115560 of ones belong to structure. However, 44370510 number of nodes and 43632000 EC3D8R type number of elements with the sizes of 0.075 m and 0.25 m are utilized in the marine environment. The mesh size is 0.075 m in the contact points of environment and the structure. However, it is taken as 0.25 m for the other parts of the environmental model.

The contacts between the Eulerian-Lagrangian parts have been discretised by using the general contact algorithm depending the penalty contact method. Explicit analysis is performed to transfer the values to fluid via CEL method. By this way, the displacement values are determined by Eq. (12).

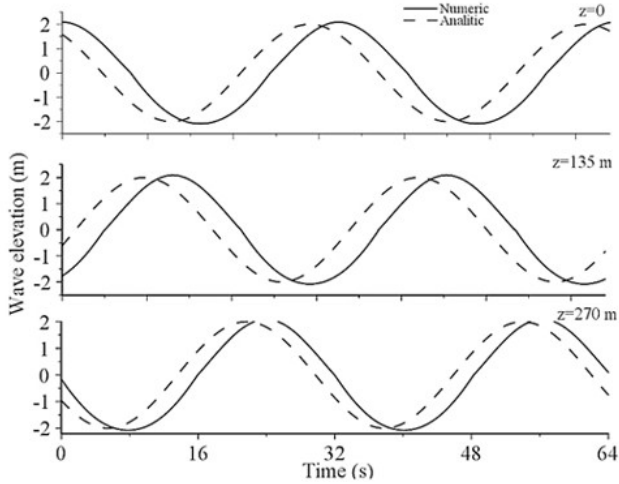
$$m^{NJ} \ddot{Z}^N|_t = (F^J - I^J)|_t \quad (12)$$

In this equation,  $m^{NJ}$  represents the mass matrix,  $\ddot{X}$  means the acceleration,  $t$  represents the time,  $F^J$  is the external applied load vector transferred from fluid flow and  $I^J$  symbolizes the internal force vector that is eventuated by stresses in the elements. Numerical analysis is generated by applying 0.01 sec of time step ( $\Delta t$ ) for 600 sec.

## 4. Results.

First of all, wave elevation of the wave ( $H=4$  m,  $T=6$  s) is determined and compared with analytical results as presented in Figure 4.

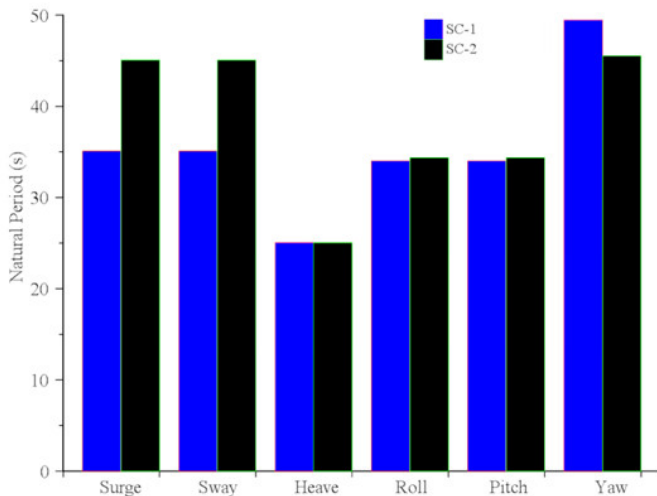
Figure 4: Wave elevations.



Source: Authors.

Entry point of the model for  $z=0$  position, analytically obtained wave elevation oscillates between  $-2.00$  m and  $+2.00$  m. Numerical values for the same position range between the range of  $-2.06$  m and  $+2.07$  m. However, while the elevation for  $z=135$  m position is analytically differs between  $-2.00$  m and  $+2.00$  m, the elevation for the same position is numerically varies between  $-2.08$  m and  $+2.09$  m. For  $z=270$  m position as the exit point of the model, analytical values oscillates between the same values just as the other positions. On the other hand, numerical values are between  $-2.07$  m and  $+2.07$  for this position. Maximum difference appears as  $\%9$  between numerical and analytical results at  $z=135$  m position.

Figure 5: Natural periods of the structure for different cases.



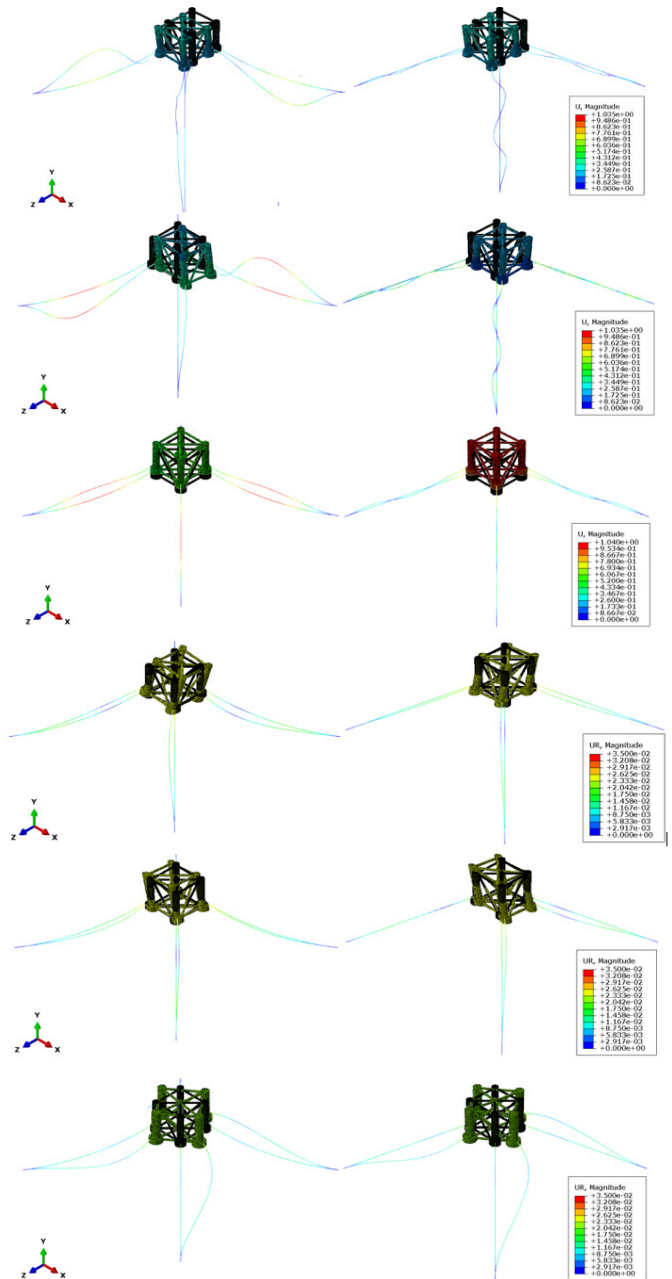
Source: Authors.

Mode shapes of the structure and the corresponding natural period values are determined by numerical analysis via Lanczos Method. Natural periods of the structure in all six modes of motion are given in Figure 5 for SC-1 and SC-2. Surge, sway,

heave, roll, pitch, and yaw natural frequency values for SC-1 are 35.08 s, 35.08 s, 25.06 s, 34.02 s, 34.02 s and 49.46 s respectively. These values are obtained as 45.07 s, 45.07 s, 25.06 s, 34.36 s, 34.36 s and 45.52 s for SC-2 in the same order.

Shapes of the six modes of the structure are visually seen in Figure 6. Whereas the translational displacements are in meters, the rotational displacements are in degrees in this figure.

Figure 6: Mode shapes and corresponding natural frequencies of the structure.

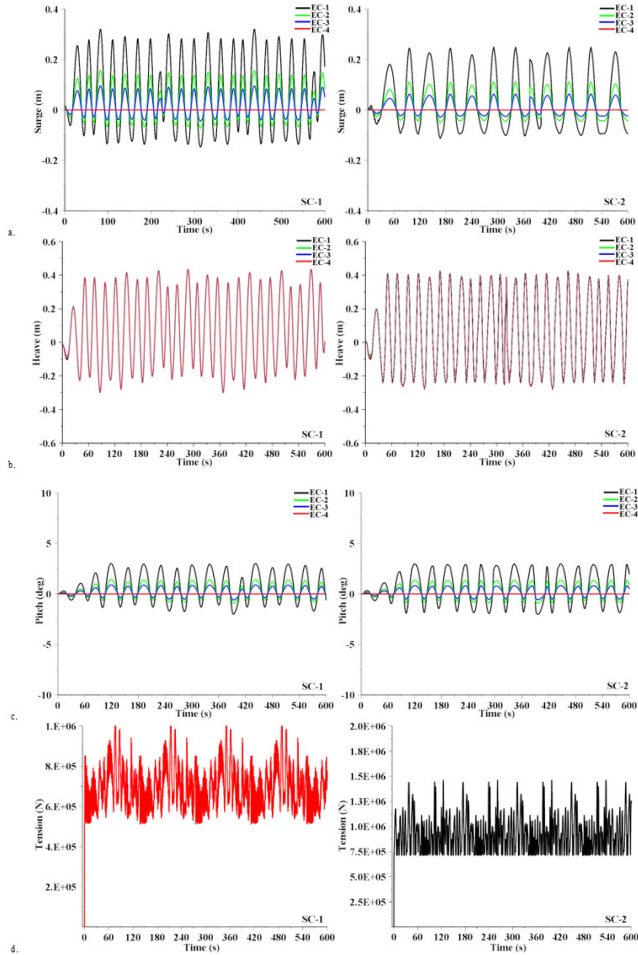


Source: Authors.

Surge, heave, and pitch motions of the floating platform are known to be the most apparent motions. Thus these three of them are chosen to investigate among six modes. Because of

the symmetry in geometry, it is clear that the motions of the surge/sway and roll/pitch complete each other for 0° and 90° incident angles. Heave, surge and pitch motions of the structure and maximum tension of the mooring lines are comparatively obtained by the structural and environmental cases, and presented in Figure 7.

Figure 7: Motions of the structure and maximum tension of the mooring lines by time.



Source: Authors.

The surge/roll and sway/pitch axes are determined as X and Y. The values of heave, surge, pitch motions and tensions of the mooring lines are presented in Table 4 for EC-1.

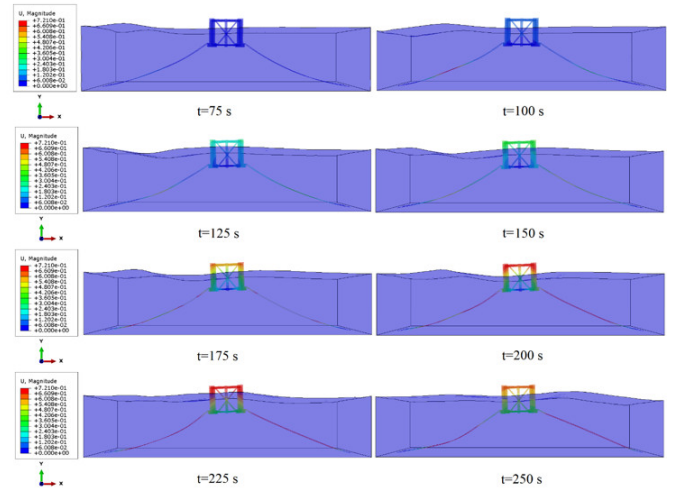
Table 4: Statistical values of structural outputs.

Outputs	Surge (m)		Heave (m)		Pitch (deg)		Tension (N)	
	SC-1	SC-2	SC-1	SC-2	SC-1	SC-2	SC-1	SC-2
Minimum	-0.14	-0.11	-0.30	-0.28	-2.08	-2.02	$5.12 \times 10^5$	$7.13 \times 10^5$
Maximum	+0.32	0.24	0.44	0.42	3.01	2.97	$1.05 \times 10^6$	$1.46 \times 10^6$
Mean	0.06	0.04	0.07	0.06	0.73	0.69	$6.98 \times 10^5$	$9.37 \times 10^5$
Standard deviation	0.14	0.12	0.21	0.22	1.49	1.64	$1.08 \times 10^5$	$1.71 \times 10^5$

Source: Authors.

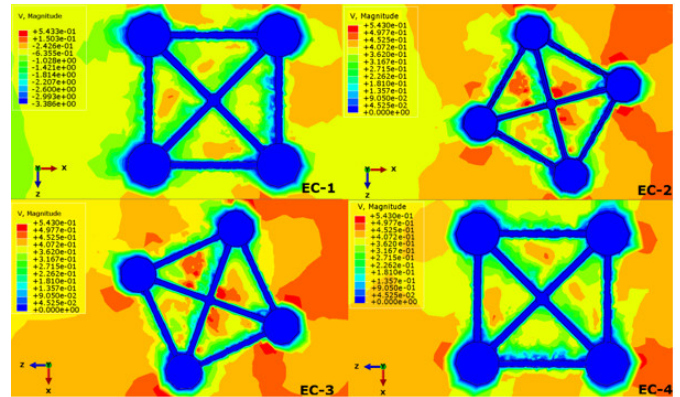
Coupled motions of the system are shown in Figures 8-9. Coupled motions of the slack mooring lines, floating structure and marine environment are seen in Figure 8 for different time periods. Velocity contours of environmental cases around base column of SC-2 are seen in Figure 9.

Figure 8: Velocity distribution of underwater pipe model.



Source: Authors.

Figure 9: Velocity contours of environmental cases.



Source: Authors.

**Conclusions.**

The fluid-structure interaction analysis of four column semi-submersible platform has been carried out in this study by utilizing CEL technique that enables to model free surface motion. As present model located on the free surface, it is crucial to examine surface movement. First of all, the numerical analysis is generated via wave surface profile. The biggest difference between numerical and analytical results of surface elevation is calculated as 9.0%. So, accordance of water surface profiles has been verified. Only wave model is performed without placing the structure in the validation phase of wave profiles. Water surface profiles are obtained for the determined two points. It is stated that the comparison between numerical and analytical

methods would not give reliable results owing to the deterioration of flow structure as the structure is placed inside.

As stated in the literature long natural period of examined model, preferably longer than 25~30 sec, to realize small motions in all six modes of motion. As it is seen from Figure 5 natural periods of both SC-1 and SC-2 are above limit values. Due to the symmetry of the structure, the natural frequency values of surge, sway, roll and pitch motions are same for each rope type. In surge and sway motions, the natural period of SC-2 is 28.5% bigger than SC-1. On the other hand, the natural period of SC-2 is 7.95% less than SC-1 in yaw motions. Mooring system has a little impact on the natural periods of heave, roll and pitch degrees of freedom.

Effect of wave directions on the floater motions are investigated in environmental cases. Time histories of heave, surge and pitch motions of the structural cases are comparatively determined according to EC-1 to EC-4. According to Figure 7 surge motion is distinctly affected by both wave direction and type of the mooring line. Surge motions in EC-1 and EC-4 are complementary to each other due to symmetrical geometry of the structure. Maximum value of the mentioned motion in SC-1 is 0.32 m, in SC-2 is 0.249 m. Heave motion is not influenced by neither environmental cases nor structural cases as the buoyancy of the platform is greater than the self-weight. It can be seen in Figure 7 that the pitch movement is affected by environmental cases, but is only affected by structural cases at a rate of 1.05%. More critical results are obtained in SC-1 and EC-1 by surge, heavy and pitch motions. Furthermore, maximum mooring line tension value is occurred in SC-2 where taut mooring lines are used.

It is seen by Figure 8 that the maximum displacement is achieved during the time period when the wave peak has approached to the structure. Visual results have revealed that the wave has not passed over the structure and caused a sinking effect on the structure. The importance of using the CEL technique, in which free surface modelling is performed is seen in this case.

Combination of structural and environmental cases on the structural behaviour of the floating structure is obtained in the scope of this study. In future studies, numerical analysis will be carried out for different rope configurations. Constant wave height and period has been used in environmental cases. Generating environmental cases for different wave heights and periods and irregular waves will be the subject of future studies. With all that cost analysis of structural cases will also be studied in further studies.

As a conclusion, motion responses are within limits for both structural and environmental cases. Although more tension occurs in rope type ropes, it is thought to be more advantageous to use SC-2 for the environment examined in the study, for reasons such as ease of supply and lightness, as it remains below the limit values. Finally, it is considered that this study is a significant step toward to the development of design of moored floating structures and the findings of the study will be useful for the researchers studying the behaviour of pontoon type structures under various cases numerically.

## References.

- Han, J. et al. (2020) 'Development of self-floating fibre reinforced polymer composite structures for photovoltaic energy harvesting', *Composite Structures*, 253 (43), 112788. doi: 10.1016/j.compstruct.2020.112788.
- Xu, S. et al. (2021) 'A novel conceptual design of a dynamically positioned floating wind turbine', *Ocean Engineering*, 221, pp. 265–276. doi: <https://doi.org/10.1016/j.oceaneng.2020.108528>.
- Chandrasekaran, S. and Sricharan, V.V.S. (2020) 'Numerical analysis of a new multi-body floating wave energy converter with a linear power take-off system', *Renewable Energy*, 159, pp. 250-271. doi: <https://doi.org/10.1016/j.renene.2020.06.007>.
- Ji, C. et al. (2016) 'Experimental study on configuration optimization of floating breakwaters', *Ocean Engineering*, 117, pp. 302–310. doi: <https://doi.org/10.1016/j.oceaneng.2016.03.002>.
- Jin, J. et al. (2021), 'Numerical modelling of hydrodynamic responses of Ocean Farm 1 in waves and current and validation against model test measurements', *Marine Structures*, 78, 103017. doi: <https://doi.org/10.1016/j.marstruc.2021.103017>.
- Xia, S. et al. (2019) 'Multivariable oscillation control of a modularized floating airport with disturbance of uncertain waves', *Journal of Sound and Vibration*, 439, pp. 310-328. doi: <https://doi.org/10.1016/j.jsv.2018.10.006>.
- Manisha, Kaligatla, R. B. and Sahoo, T. (2019) 'Effect of bottom undulation for mitigating wave-induced forces on a floating bridge', *Wave motion*, 89 pp. 166-184. doi: <https://doi.org/10.1016/j.wavemoti.2019.03.007>.
- Aboshio, A. and Ye, J. (2016) 'Numerical study of the dynamic response of in-table offshore fender barrier structures using the Coupled Eulerian–Lagrangian discretization technique', *Ocean Engineering*, 112, pp. 265–276. doi: <https://doi.org/10.1016/j.oceaneng.2015.12.020>.
- Chungkuk, J., Bakti, F. P. and Kim, M. (2020) 'Multi-floater-mooring coupled time-domain hydro-elastic analysis in regular and irregular waves', *Applied Ocean Research*, 101, 102276. doi: <https://doi.org/10.1016/j.apor.2020.102276>.
- Gomes, R.P.F. et al. (2020) 'Compact floating wave energy converters arrays: Mooring loads and survivability through scale physical modelling', *Applied Energy*, 280, 115982. doi: <https://doi.org/10.1016/j.apenergy.2020.115982>.
- Huang, X. et al. (2020) 'Hydrodynamic performance of a semi-submersible offshore fish farm with a single point mooring system in pure waves and current', *Aquacultural Engineering*, 90, 102075. doi: <https://doi.org/10.1016/j.aquaeng.2020.102075>.
- Yuan, Z.M., Incecik, A. and Ji C. (2014) 'Numerical study on a hybrid mooring system with clump weights and buoys', *Ocean Engineering*, 88, pp. 1–11. doi: <https://doi.org/10.1016/j.oceaneng.2014.06.002>.
- Qiao, D., et al. (2020) 'Analysis on snap load characteristics of mooring line in slack-taut process', *Ocean Engineering*, 196, doi: <https://doi.org/10.1016/j.oceaneng.2019.106807>.
- Chung, W.C., Kang, H.Y. and Kim, M.H. (2020) 'Multi-scale approach for chain-mooring OPB-induced failure consid-

ering time-varying interlink bending stiffness and fairlead condition', *Applied Ocean Research*, 98, 102128. doi: <https://doi.org/10.1016/j.apor.2020.102128>.

Hermawan, Y.A. and Furukawa, Y. (2020) 'Coupled three-dimensional dynamics model of multi-component mooring line for motion analysis of floating offshore structure', *Ocean Engineering*, 200, 106928. doi: <https://doi.org/10.1016/j.oceaneng.2020.106928>.

Li, X. et al. (2020) Effects of the yaw error and the wind-wave misalignment on the dynamic characteristics of the floating offshore wind turbine, *Ocean Engineering*, 199, 106960, doi: <https://doi.org/10.1016/j.oceaneng.2020.106960>.

Chen, M., Chen, J. and Yun-Xiang, Y. (2020) 'Forces on a semi-submersible in internal solitary waves with different propagation directions', *Ocean Engineering*, 217, 107864. doi: <https://doi.org/10.1016/j.oceaneng.2020.107864>.

Zhou, S. et al. (2017) 'Directionality effects of aligned wind and wave loads on a y-shape semi-submersible floating wind turbine under rated operational conditions', *Energies*, 12, 2097. doi: <https://doi.org/10.3390/en10122097>.

Wiegard, B. et al. (2019) Simulation of the fluid-structure interaction of a floating wind turbine, *Ships and Offshore Structures*, 14, pp. 207-218. doi: <https://doi.org/10.1080/17445302.2019.1565295>.

Chen, X. et al. (2017) 'Numerical and experimental analysis of a moored pontoon under regular wave in water of finite depth', *Ships and Offshore Structures*, 12(3), pp. 412–423. <https://doi.org/10.1080/17445302.2016.1172831>

Ji, C. et al. (2017) 'Numerical and experimental investigation of hydrodynamic performance of a cylindrical dual pontoon-net floating breakwater', *Coastal Engineering*, 129, pp. 1-16, doi: <https://doi.org/10.1016/j.coastaleng.2017.08.013>.

Haicheng, Z. et al. (2018) Energy extraction of wave energy converters embedded in a very large modularized floating platform, *Energy* 158 (1), pp. 317-329. doi: <https://doi.org/10.1016/j.energy.2018.06.031>.

Rajeswari, K. and Nallayarasu, S. (2021) 'Experimental and numerical investigation on the suitability of semi-submersible floaters to support vertical axis wind turbine', *Ships and Offshore Structures*, 17(8), pp. 1743-1754, doi: <https://doi.org/10.1080/17445302.2021.1938800>.

Gücüyen, E. and Erdem, R.T. (2022) 'Numerical modelling of floating structure with coupled Eulerian–Lagrangian technique', *Gradevinar*, 74 (10), pp. 869-880. doi: <https://doi.org/10.14256/JCE.3276.2021>.

ABAQUS Documentation, Version 6.12. SIMULIA, Dassault, Systèmes Simulia Corp., 2015.